ACS APPLIED MATERIALS & INTERFACES

www.acsami.org

Research Article

Di-Arginine Additives for Dissociation of Gold Nanoparticle Aggregates: A Matrix-Insensitive Approach with Applications in Protease Detection

Maurice Retout, Zhicheng Jin, Jason Tsujimoto, Yash Mantri, Raina Borum, Matthew N. Creyer, Wonjun Yim, Tengyu He, Yu-Ci Chang, and Jesse V. Jokerst*

Cite This: *ACS Appl. Mater. Interfaces* 2022, 14, 52553−52565

Read Online

ACCESS | Metrics & More | Article Recommendations | Supporting Information

ABSTRACT: We report the reversible aggregation of gold nanoparticles (AuNPs) assemblies via a di-arginine peptide additive and thiolated PEGs (HS-PEGs). The AuNPs were first aggregated by attractive forces between the citrate-capped surface and the arginine side chains. We found that the HS-PEG thiol group has a higher affinity for the AuNP surface, thus leading to redispersion and colloidal stability. In turn, there was a robust and obvious color change due to on/off plasmonic coupling. The assemblies' dissociation was directly related to the HS-PEG structural properties such as their size or charge. As an example, HS-PEGs with a molecular weight below 1 kDa could dissociate 100% of the assemblies and restore the exact optical properties of the initial AuNP suspension (prior to the assembly). Surprisingly, the dissociation capacity of HS-PEGs was not affected by the composition of the operating medium and could be performed in complex matrices such as plasma, saliva, bile, urine, cell lysates, or even seawater. The high affinity of thiols for the gold surface encompasses by far the one of endogenous molecules and is thus favored. Moreover, starting with AuNPs already aggregated ensured the absence of a background signal as the dissociation of the assemblies was far from spontaneous. Remarkably, it was possible to dry the AuNP assemblies and solubilize them back with HS-PEGs, improving the colorimetric signal generation. We used this system for protease sensing in biological fluids. Trypsin was chosen as the model enzyme, and highly positively charged peptides were conjugated to HS-PEG molecules as cleavage substrates. The increase of positive charge of the HS-PEG−peptide conjugate quenched the dissociation capacity of the HS-PEG molecules, which could only be restored by the proteolytic cleavage. Picomolar limit of detection was obtained as well as the detection in saliva or urine.

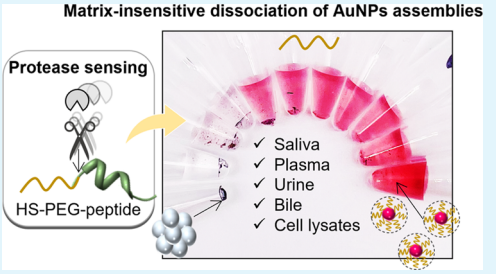

KEYWORDS: *gold nanoparticles, reversible assembly, protease sensing, colorimetric detection, PEG, peptides*

INTRODUCTION

Noble nanomaterials and particularly gold nanoparticles (AuNPs) have emerged as remarkable colorimetric reporters due to their plasmonic properties.[1−3] AuNPs possess a localized surface plasmon resonance (LSPR) band in the visible region that is modulated by their size, shape, and dielectric environment.[4−6] Citrate-capped AuNPs (AuNPs−citrate) are the most common, convenient, and cost-effective form of gold colloids, and their synthesis *via* the Turkevich method is well established in the literature.[7] AuNPs have been extensively studied, and various AuNP-based colorimetric sensors have been developed.[8−10]

One attractive and common sensing/analysis strategy with AuNPs is the cross-linking of the particles induced by the analyte that couple individual LSPR bands, thus shifting the initial red color of the dispersed AuNPs to blue as the distance between particles diminishes.[8,11,12] Different mechanisms have been thus exploited to induce the assembly of AuNPs such as DNA pairing,[13] antibody−antigen interactions,[10] electrostatic interactions,[8] and hydrogen bonding.[14]

However, one limitation is their colloidal stability. Indeed, their dispersibility is inherent to the balance of attractive van der Waals (VdW) and repulsive electrostatic forces.[15] Thermodynamically, AuNP colloids are not stable and tend to aggregate over time, which results in the nondesired aggregation of the particles that reduces the color difference between a positive sample (analyte present) and a negative sample (analyte absent).[8,16] Another limitation is the difficulty to operate in biofluids such as plasma, saliva, urine, bile, or cell lysates. The presence of background matrix compounds can interfere with the colorimetric detection, e.g., via a protein corona that prevents the AuNP cross-linking.[17] Also, dramatic background signals are usually observed in biofluids because there is

Received: September 28, 2022
Accepted: October 21, 2022
Published: November 8, 2022

Scheme 1. Assembly of Citrate-Capped AuNPs (AuNPs−Citrate) with a Di-Arginine Peptide and Subsequent Dissociation with Thiolated PEG Molecules (HS-PEGs)

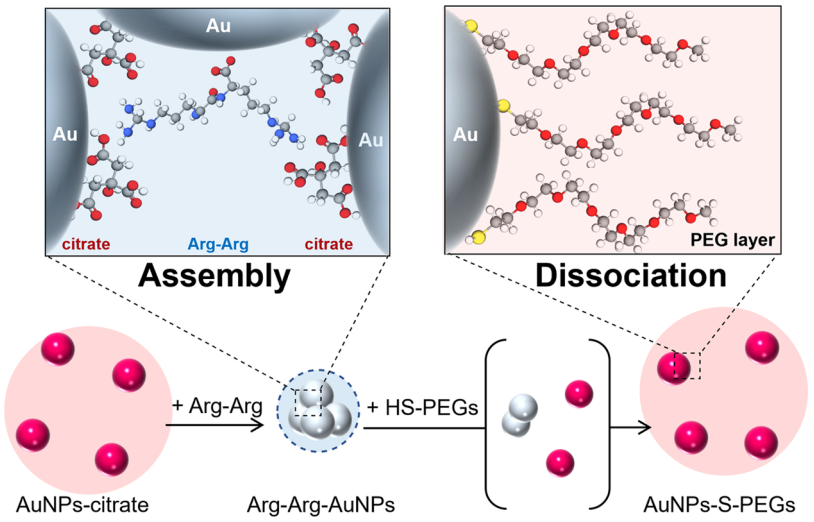

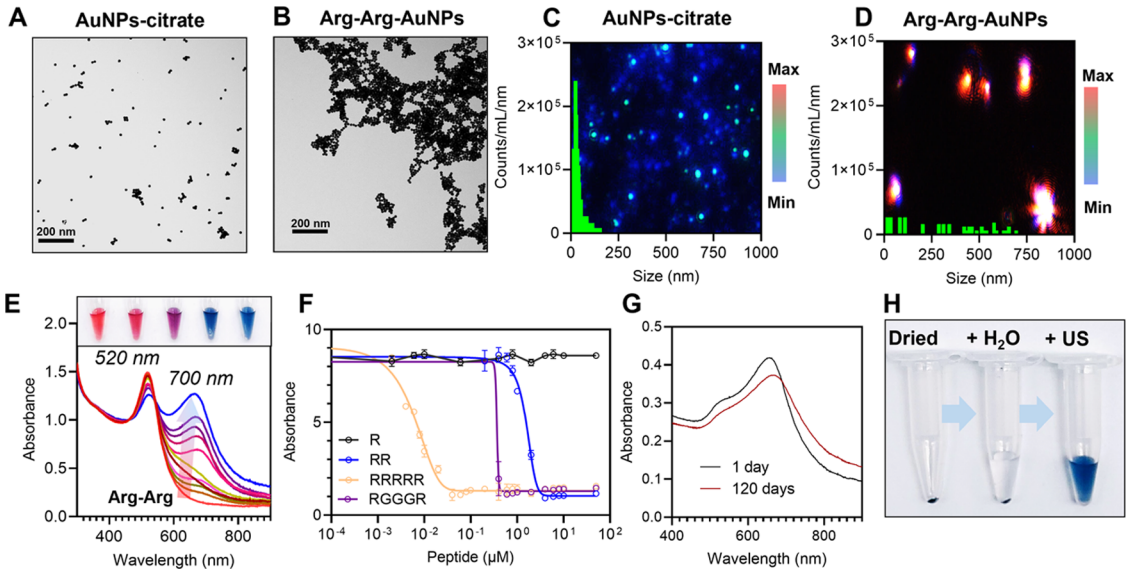

Figure 1. Peptide-induced assembly of AuNPs−citrate. (A−D) TEM images and multispectral advanced nanoparticle tracking analysis (MANTA)[29] image and size distribution of AuNPs−citrate before (A, C) or 10 min after the addition of 10 μM of Arg−Arg (B, D). MANTA records images of the particles' light scattering via three differently colored lasers (e.g., blue, green, and red); the scattering depends on the particle's size. MANTA counts the nanoparticles and calculates their size. (E) Modification of the optical properties of AuNPs−citrate during the assembly with Arg−Arg. Insets show the pictures of the samples for concentrations of Arg−Arg of 0, 1, 2, 5, and 10 μM. (F) Ratio of the absorbances $Abs._{520nm}/Abs._{700nm}$ of AuNPs−citrate as a function of peptide concentration. (G) UV−vis spectra of Arg−Arg−AuNPs 1 day or 120 days old. (H) Pictures of Arg−Arg−AuNPs dried and resuspended in pure water after 5 s of sonication.

significant charge screening, thus leading to a reduction in repulsive forces and aggregation of the AuNPs due to the VdW interaction. Extreme dilution of the biological sample[16] or extraction of the analyte from the matrix is thus often needed.[18] Only a few examples of nanoparticle aggregation-based assays in biological fluids have been reported.[19,20]

Here, we show a novel process of reversible aggregation of AuNPs−citrate for alternative sensing strategies. Reversible aggregation of nanoparticles is challenging because, according to the Derjaguin−Landau−Verwey−Overbeek (DLVO) theory,[21] the particles can be trapped in deep energetic minima during the aggregation, thus transforming the aggregates into larger insoluble materials that can be only slightly dissociated by aggressive sonication; their optical properties cannot be recovered.[22] While many in the community have shown the reversible assembly of a small number of nanoparticles, this usually requires sophisticated coating of the AuNP-citrate surface with responsive polymers,[23,24] DNA strands,[25,26] or other organic ligands.[27,28] However, we are unaware of work describing the assembly of a large amount of AuNPs−citrate into macroscopic aggregates that can easily be dissociated without the need for prior surface modifications.

Our system uses only a di-arginine additive that causes the aggregation of AuNPs and thiolated poly(ethylene glycol) (HS-PEG) for the dissociation of the assemblies (Scheme 1). The system works through differences in affinity of the surface ligands: the introduction of HS-PEGs leads to the redispersion of the AuNPs due to the higher affinity of the thiol for the gold

https://doi.org/10.1021/acsami.2c17531
ACS Appl. Mater. Interfaces 2022, 14, 52553−52565

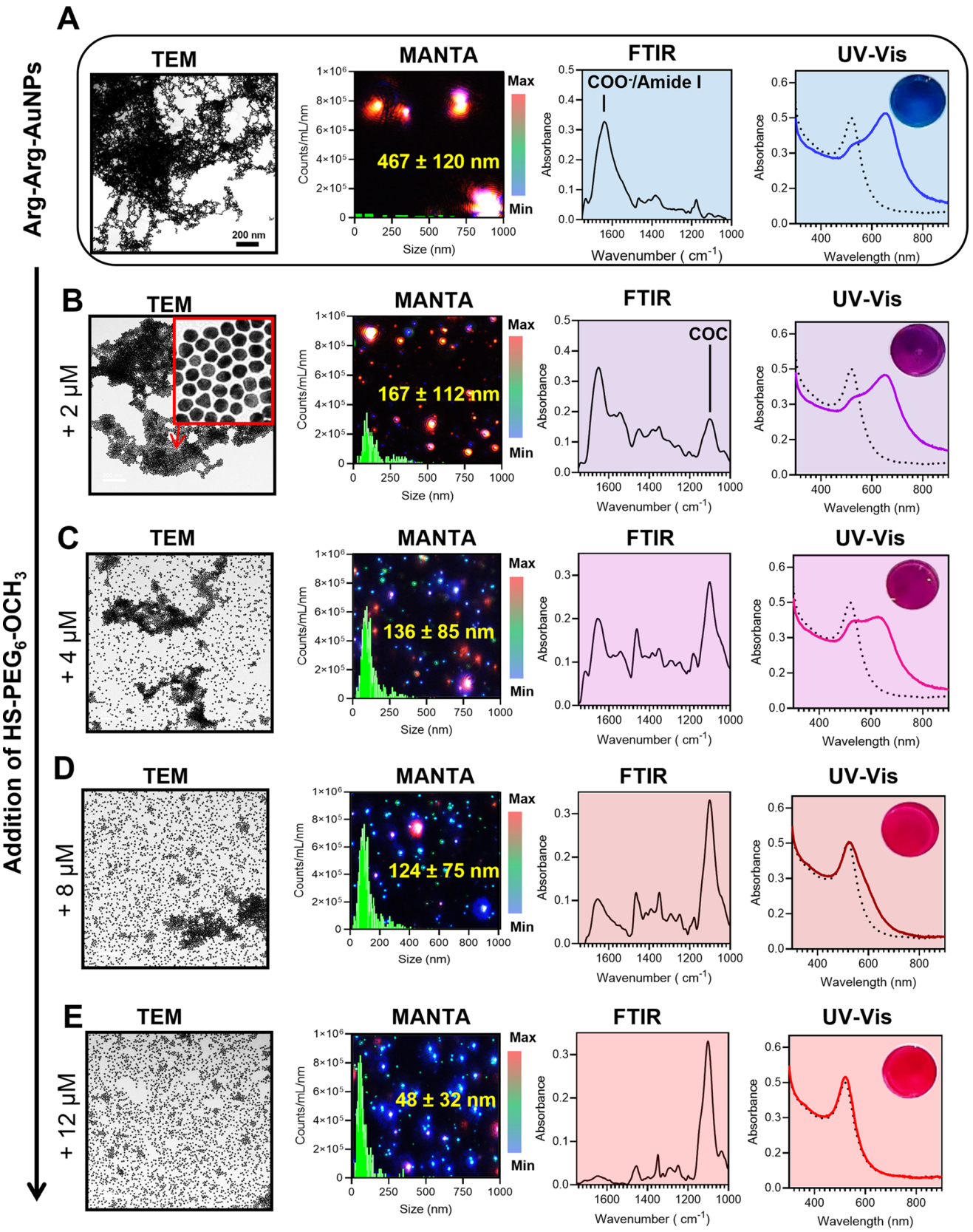

Figure 2. Characterization of the dissociation of AuNP assemblies with HS-PEG_6-OCH_3. From left to right, TEM*, MANTA, ATR-FTIR**, and UV−vis*** spectroscopy analyses of Arg−Arg−AuNPs (A) before or 10 min after the addition of (B) 2 μM, (C) 4 μM, (D) 8 μM, and (E) 12 μM of HS-PEG_6-OCH_3. *All of the images are at the same magnification. **All samples were cleaned by centrifugation from nonbound molecules (HS-PEGs, citrate, or Arg−Arg), and the FTIR spectrum corresponds only to molecules attached to the gold surface. *** The black dashed line shows the LSPR band of the initial AuNPs−citrate.

https://doi.org/10.1021/acsami.2c17531
ACS Appl. Mater. Interfaces 2022, 14, 52553−52565

surface than the arginine or citrate. In turn, there is a plasmonic color change. Starting with assembled AuNPs allows for insight into the colorimetric signal. Surprisingly, the redispersion can be performed over a wide variety of solvents including human plasma, serum, saliva, and even bile. After characterizing the ligands and HS-PEGs best suited for this reaction, we deployed it for colorimetric sensing of proteases via a cleaved PEG−peptide conjugate. Although the grafting of HS-PEG molecules on dispersed AuNPs has been widely reported in the literature, to the best of our knowledge, the dissociation of AuNP assemblies with HS-PEGs has never been studied before, especially for the detection of proteases.

RESULTS AND DISCUSSION

Formation of AuNP Assemblies. In this study, we investigated the possibility of forming convenient and reversible AuNP assemblies using only elementary 15 nm AuNPs−citrate suspended in water and short peptides without the need for a complex surface modification. Peptides were used because they are relatively bulky and thus their steric prevented the particles from entering a permanent aggregated state. Arginine, in particular, can strongly interact with citrate anions via electrostatic interactions. A dipeptide containing two repetitions of arginine (Arg−Arg or RR) was thus used to interact with multiple particles at the same time and induce assembly.

Transmission electronic microscopy (TEM) revealed that the addition of excess (10^4 equiv) of di-arginine peptide (Arg−Arg) to an aqueous suspension of AuNPs−citrate led to bulky assemblies, and no dispersed AuNPs were observed (Figure 1A,B). Multispectral advanced nanoparticle tracking analysis (MANTA) was then used to confirm the size increase: the initial blue scattering corresponding to a hydrodynamic diameter of 40 ± 25 nm (Figure 1C) transformed immediately into red scattering corresponding to a hydrodynamic diameter of approximately 467 ± 120 nm (Figure 1D). Importantly, the count of particles decreased by more than 90%—from 2.5×10^5 to 2×10^4/mL, thus confirming that the vast majority of the AuNPs−citrate were aggregated. TEM images at different magnifications are seen in the Supporting Information (Figures S1 and S2).

The peptide-induced assembly of AuNPs−citrate strongly impacted the optical properties of the colloid. An immediate modification of the LSPR band of the particles was observed proportional to the peptide concentration. The absorbance at λ_{max} decreased, and a new absorption peak increased at 700 nm (Figure 1E). Such deformation of the LSPR band led to a change of color of the suspensions turning from bright red to blue (Figure 1E, insets). The ratio of the absorbance at 520 over 700 nm was then used to characterize the AuNP assemblies throughout this study. Interestingly, the density of Arg−Arg leading to the maximal ratio of absorbance was approximately 1.8 Arg−Arg-/nm^2, which corresponds approximately to the maximal density of Arg−Arg that could be carried out by one AuNPs (1.6 Arg−Arg/nm^2) considering a footprint for the peptide of 0.63 nm^2 (see http://biotools.nubic.northwestern.edu/proteincalc.html).

Arg−Arg was chosen to promote the AuNP-citrate assemblies because it is the minimal sequence that can induce the assembly. The reversibility of our system is based on the replacement of citrate and peptide layers by PEG, and it was thus crucial to remove the peptides from the AuNP surface. While a single arginine could not induce any form of assembly, peptides containing more than two arginines had a higher affinity for the AuNPs−citrate than Arg−Arg and were thus discarded (Figure 1F). As a control, we synthesized a peptide containing two arginines but spaced by three glycines (RGGGR) to decrease the charge density and thus lower the affinity of the peptide for the AuNPs−citrate. However, RGGGR had a higher affinity for the particles than RR (Arg−Arg) and was also discarded.

Despite its short length, Arg−Arg was sufficient to protect the AuNPs from degradation, and the resulting assemblies were highly stable over time. Figure 1G shows barely any difference between the LSPR band of pristine and 120 day old Arg−Arg−AuNPs. To our delight, another demonstration of the high stability of the assemblies was performed with their drying and resuspension in pure water using only 5 s of sonication without any degradation or loss of particles (Figure 1H).

To demonstrate the versatility of our system, this study was reproduced with 40 nm of AuNPs−citrate commercially available from Nanocomposix (Supporting Information Section 7).

Dissociation of the AuNP Assemblies. The proof of concept of the assembly reversibility was demonstrated with a poly(ethylene glycol) (PEG) system containing six repetitions capped with a methoxy group and a thiol at the other end (HS-PEG_6-OCH_3). HS-PEG_6-OCH_3 was chosen because its grafting on AuNPs ensures a high colloidal stability of the latter. Indeed, the grafting of thiolated PEGs has been widely reported in the literature via the formation of a strong Au−S bond, conferring to the particles a high colloidal stability due to a combination of hydrophilicity and steric hindrance.[30−32] The Au−S bond being stronger than the arginine−citrate, arginine−gold, or even citrate−gold interactions, HS-PEG_6-CH_3 was expected to be capable of progressively replacing the arginine/citrate layers at the gold surface, disrupting the electrostatic network and eventually dispersing the AuNPs (Scheme 1). Briefly, aqueous suspensions of Arg−Arg−AuNP assemblies were exposed to increasing concentrations of HS-PEG_6-OCH_3, and the dissociation of the assemblies was characterized by TEM, MANTA, FTIR, and UV−vis spectroscopies (Figure 2).

Prior to any addition of HS-PEGs, the dense and large aggregates of Arg−Arg−AuNPs present only ATR-FTIR signals coming from citrate and/or Arg−Arg as well as $COO^-_{\nu as}$ and/or amide band I around 1650 cm^{-1}, respectively. The color of the sample was bright blue because the LSPR band was strongly red-shifted (Figure 2A).

After the addition of 2 μM of HS-PEG_6-OCH_3, however, the distance between the AuNPs in the aggregates increased and the size of the aggregates decreased from 467 ± 120 to 167 ± 112 nm. Interestingly, ATR-FTIR spectroscopy showed an increase in the absorbance at 1100 cm^{-1} corresponding to the C−O−C stretching of the PEG chain and a decrease in the absorbance around 1650 cm^{-1}. This indicates that a few HS-PEG_6-OCH_3 were grafted onto the AuNP surface, which explains the increase in the interparticle distance. The decrease in the size of the assembly led to a color change from blue to purple (Figures 2B and S3).

Figure 2C,D shows the results of the addition of 4 and 8 μM of HS-PEG_6-OCH_3, respectively. More AuNPs detached from the aggregates and became monodisperse with higher concentrations of HS-PEG_6-OCH_3 (Figures S4 and S5). Accordingly, the average size of the aggregates decreased to 136 ± 85 and 124 ± 75 nm for 4 and 8 μM, respectively. Moreover, the intensity of the ATR-FTIR signals of the PEG chain increased and the signal of the citrate/Arg−Arg decreased, thus confirming the expansion of the grafting density of HS-PEG_6-OCH_3. The

https://doi.org/10.1021/acsami.2c17531
ACS Appl. Mater. Interfaces 2022, 14, 52553−52565

LSPR band of the colloid red-shifted due to dissociation: the solution color was purple-pink and wine red at 4 and 8 μM, respectively.

At 12 μM of HS-PEG$_6$-OCH$_3$ and above, aggregates were no longer seen in TEM, and MANTA measured a mean size of 48 ± 25 nm. ATR-FTIR showed only absorbance of the C−O−C signal with limited citrate/Arg−Arg signals, thus indicating that the citrate/arginine layer was completely removed from the surface for the benefit of HS-PEG$_6$-OCH$_3$. The presence of a PEG layer around the AuNPs explains the difference in the hydrodynamic diameter versus the initial AuNPs−citrate (48 ± 32 vs 40 ± 25 nm). Remarkably, the LSPR band of the dissociated AuNPs was identical to the AuNPs−citrate: the color of the sample returned to its initial bright red color. This suggests that 100% of the aggregates was dissociated and that all AuNPs were detached and dispersed. For the remainder of this study, the efficiency of the dissociation will be characterized by the percentage of dissociation (%), as measured by UV−vis spectroscopy (comparison between the LSPR band after dissociation versus that from AuNPs−citrate) (see the Experimental Section in the Supporting information for more details). Importantly, a concentration of 12 μM corresponds to a density of ∼4 HS-PEG$_6$-OCH$_3$/nm^2. This finding is particularly interesting because the typical grafting density of HS-PEG$_6$-OCH$_3$ on dispersed AuNPs is reported to be between 3.5 and 4 HS-PEG$_6$-OCH$_3$ /nm^2.[33] This implies that no excess of HS-PEGs was needed to dissociate the entire assembly—only enough to cover all of the gold surfaces. It is worth noting that the kinetics of the dissociation was almost instantaneous (equilibrium reached within 10 min) (Figure S6). A video of the dissociation of the AuNP assemblies is available online.

These findings suggest that HS-PEG$_6$-OCH$_3$ can penetrate the assembly and graft onto the AuNP surface, thus displacing the citrate and arginine layer. The particle becomes sterically stabilized and water-soluble when a sufficient amount of HS-PEG$_6$-OCH$_3$ is grafted on the particle surface; thus, the particle detaches from the assembly. When the concentration of HS-PEG$_6$-OCH$_3$ is sufficiently high to cover all of the particle surfaces, all assemblies dissociate, and the optical properties of the AuNPs are restored to those of the initial dispersed AuNPs−citrate. This phenomenon is possible only because (i) the AuNPs are not trapped in the permanent aggregated state and (ii) HS-PEG$_6$-OCH$_3$ can replace the citrate/arginine layers due to the covalent grafting onto the gold surface.

To demonstrate the necessity of these two features, multiple control experiments were conducted. First, peptide-free conditions were used to promote the assembly of AuNPs−citrate and its dissociation with HS-PEG$_6$-OCH$_3$ was evaluated (Figure 3A). Here, salts were added to AuNPs−citrate to induce aggregation via disruption of the electrostatic repulsion forces between the particles. Even the addition of a high concentration of HS-PEG$_6$-OCH$_3$ (>100 μM) could not dissociate the assemblies, and the color of the samples remained dull blue/gray. Unlike the peptide Arg−Arg, these ions cannot sterically prevent the AuNPs from falling into an irreversible aggregated state.

AuNPs with different coating ligands were also evaluated and compared to citrate: bis(p-sulfonatophenyl)phenylphosphine (BSPP), mercaptobenzoic acid (MBA), or thiolated PEG-COOH (HS-PEG-COOH; Mw = 634 g.mol^{-1}). Similar to the AuNPs−citrate, the presence of Arg−Arg led to the assembly of AuNPs−BSPP, AuNPs−MBA, and AuNPs−S-PEG-COOH. However, only the AuNPs−BSPP could be dissociated;

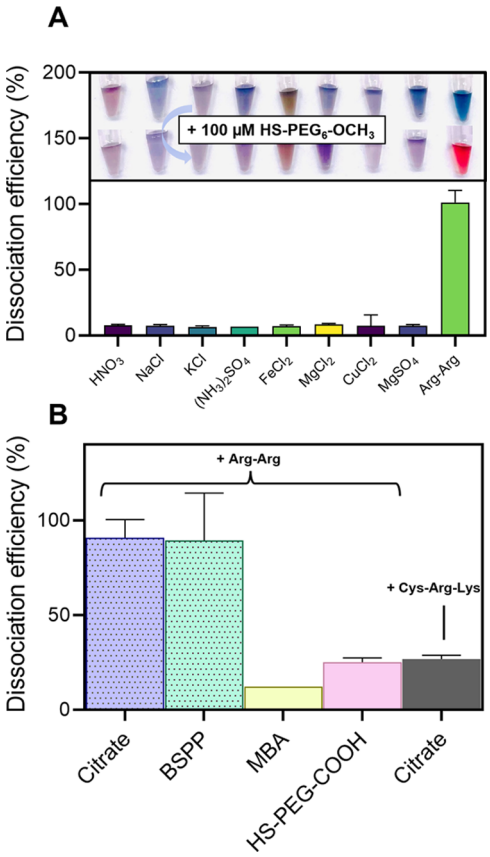

Figure 3. Dissociation efficiency of HS-PEG$_6$-OCH$_3$ for alternative assembly conditions or coating ligands. (A) Dissociation efficiency of 100 μM of HS-PEG$_6$-OCH$_3$ added to AuNPs−citrate assembled in peptide-free conditions. (B) Dissociation efficiency of 100 μM of HS-PEG$_6$-OCH$_3$ added to either AuNPs−citrate, AuNPs−BSPP, AuNPs−MBA, or AuNPs−S-PEG-COOH assembled with 10 μM of Arg−Arg or AuNPs−citrate assembled with 10 μM of Cys−Arg−Lys peptide.

assemblies of AuNPs−MBA or AuNPs−S-PEG-COOH were irreversible even in the presence of high concentrations (>100 μM) of HS-PEG$_6$-OCH$_3$ (Figure 3B). This is because MBA and HS-PEG-COOH make covalent Au−S bonds with the gold surface that prevent subsequent grafting of HS-PEG$_6$-OCH$_3$. In contrast, BSPP, like citrate, is only physisorbed onto the gold surface and can be easily displaced by HS-PEG$_6$-OCH$_3$, thus making the assembly reversible.

Finally, an alternative control peptide was used for assembly (Cys−Arg−Lys). This peptide could aggregate the AuNPs−citrate but the assembly was irreversible (Figure 3B). This is because this peptide can make a covalent Au−S bond with the gold surface via the cysteine, thus hindering the grafting of HS-PEG$_6$-OCH$_3$ on the AuNP surface and preventing dissociation. These control experiments show that the coating ligands as well as the aggregation peptide need to be weakly adsorbed onto the gold surface to facilitate aggregation and dissociation. Importantly, as the aggregates do not degrade over time, their dissociation was still possible even 120 days after their formation without a significant difference in the percent dissociation (Figure S7).

Effect of the PEG Structure on the Dissociation Capacity. The impact of PEG structure on dissociation capacity was studied next, i.e., ligands differing either by their size, anchoring group, core, or charge (Table 1).

https://doi.org/10.1021/acsami.2c17531
ACS Appl. Mater. Interfaces 2022, 14, 52553−52565

Table 1. Summary of the Ligands Used to Dissociate the AuNP Assemblies

description	name	Mw ($g \cdot mol^{-1}$)	anchor	core	end group	dissociation (%)
effect of the anchoring group	OH-PEG_6-OCH_3	296	OH	PEG_6	methoxy	0
	Alk-PEG_4-OCH_3	232	alkyne	PEG_4	methoxy	87
	LA-PEG_{22}-OCH_3	1000	lipoic acid	PEG_{22}	methoxy	92
effect of the PEG core	MBA	154	thiol	benzene	carboxyl	0
	MPA	106	thiol	propane	carboxyl	0
effect of the charge	HS-PEG_{226}-NH_2	10,000	thiol	PEG_{226}	amine	30
effect of the PEG size	HS-PEG_{450}-OCH_3	20,000	thiol	PEG_{450}	methoxy	20
	HS-PEG_{226}-OCH_3	10,000	thiol	PEG_{226}	methoxy	35
	HS-PEG_{110}-OCH_3	5000	thiol	PEG_{110}	methoxy	60
	HS-PEG_{44}-OCH_3	2000	thiol	PEG_{44}	methoxy	75
	HS-PEG_{22}-OCH_3	1000	thiol	PEG_{22}	methoxy	91
	HS-PEG_6-OCH_3	356	thiol	PEG_6	methoxy	100
	HS-PEG_4-OCH_3	224	thiol	PEG_4	methoxy	100

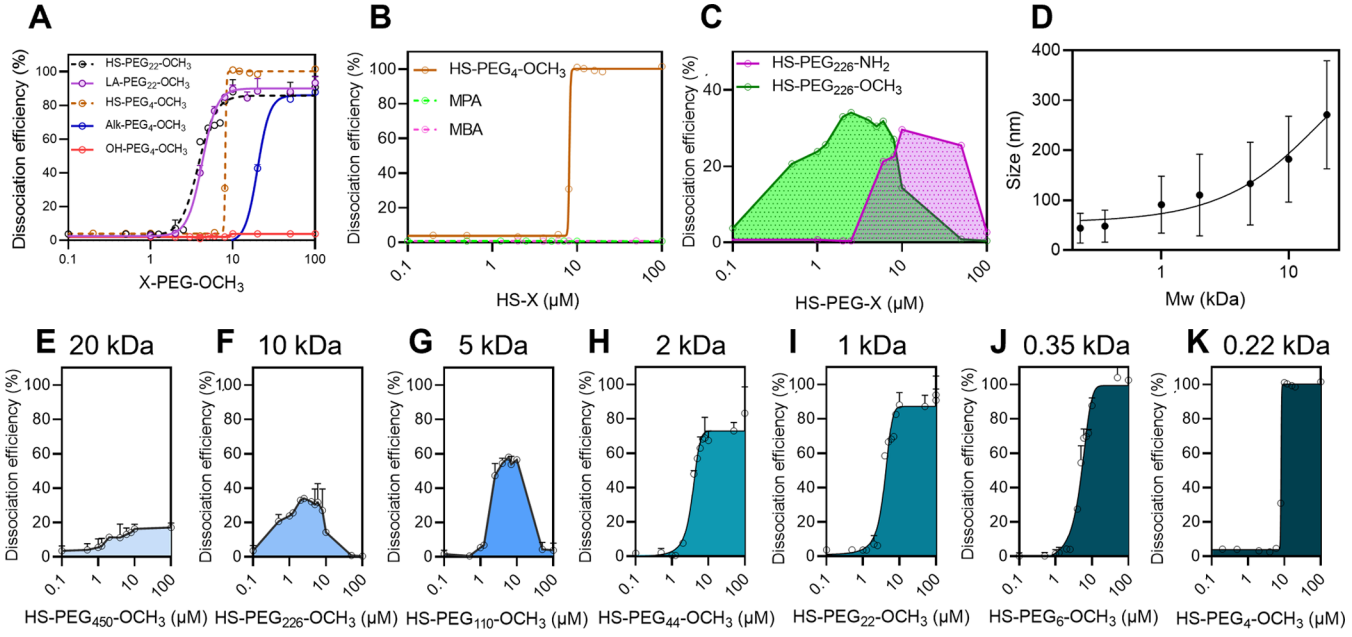

Figure 4. Effect of the PEG properties on the dissociation efficiency. (A) Dissociation efficiency of X-PEG-OCH_3 molecules carrying various anchoring groups added to Arg−Arg−AuNPs. X = thiol (HS), hydroxy (OH), lipoic acid (LA), or alkyne (Alk). (B) Dissociation efficiency of HS-PEG_4-OCH_3, MBA, or MPA added to Arg−Arg−AuNPs. (C) Dissociation efficiency of HS-PEG_{226}-OCH_3 compared to that of HS-PEG_{226}-NH_2 added to Arg−Arg−AuNPs. (D) Size of the assembly 20 min after the addition of HS-PEG_x-OCH_3 to Arg−Arg−AuNPs of different molecular weights (20, 10, 5, 2, 1, 0.35, and 0.22 kDa). (E, K). Dissociation efficiency of the HS-PEG_x-OCH_3 concentration with different molecular weights added to Arg−Arg−AuNPs.

First, to confirm that the grafting of the PEG on the AuNPs is critical to dissociation, methoxy PEG molecules carrying different anchoring groups (x-PEG-OCH_3) were studied. Figure 4A shows that the dissociation of Arg−Arg−AuNP assemblies is no longer possible when the thiol group (HS-PEG_4-OCH_3) is replaced by a hydroxy group (OH-PEG_4-OCH_3) even at high concentrations (>100 μM). This is because OH-PEG_4-OCH_3 cannot bind covalently to the gold surface. Positive controls involving alkyne (Alk-PEG_4-OCH_3) and lipoic acid (LA-PEG_{22}-OCH_3) as anchoring groups were investigated because these two chemical groups, like thiol groups, can form a covalent bond with the gold atoms at the AuNP surface.[34,35] Thus, as expected, the addition of Alk-PEG_4-OCH_3 or LA-PEG_{22}-OCH_3 led to the dissociation of the AuNP assemblies (Figure 4B). Interestingly, while LA-PEG_{22}-OCH_3 had a similar dissociation efficiency to its thiolated counterpart (HS-PEG_{22}-OCH_3), the one of Alk-PEG_4-OCH_3 was lower compared to that of HS-PEG_4-OCH_3. It can be explained by the fact that alkynes form a less labile strong bond with the surface compared to thiols. Overall, the results confirm the necessity for the dissociating ligands to be capable of grafting onto the AuNP surface.

Non-PEG ligands such as mercaptobenzoic acid (MBA) and mercaptopropionic acid (MPA) were investigated next: interestingly, none could dissociate the aggregates despite the presence of a thiol group in their structures (Figure 4B). The flexibility and hydrophilicity of the PEG chain are likely crucial to make the AuNPs water-soluble and detach them from the bulky and hydrophobic aggregate.

Finally, we demonstrated that the charge and the size of the PEG molecules have a strong impact on their capacity to dissociate AuNP aggregates. Figure 4C shows that the dissociation of HS-PEG_{226}-OCH_3 is strongly affected when the methoxy group is replaced by an amine group (net charge = +1). The effect of the size of the PEG molecule was then studied using various HS-PEGx-OCH_3 of different molecular weights ranging from 20 to 0.22 kDa. Figure 4D shows that the size of the

https://doi.org/10.1021/acsami.2c17531
ACS Appl. Mater. Interfaces 2022, 14, 52553−52565

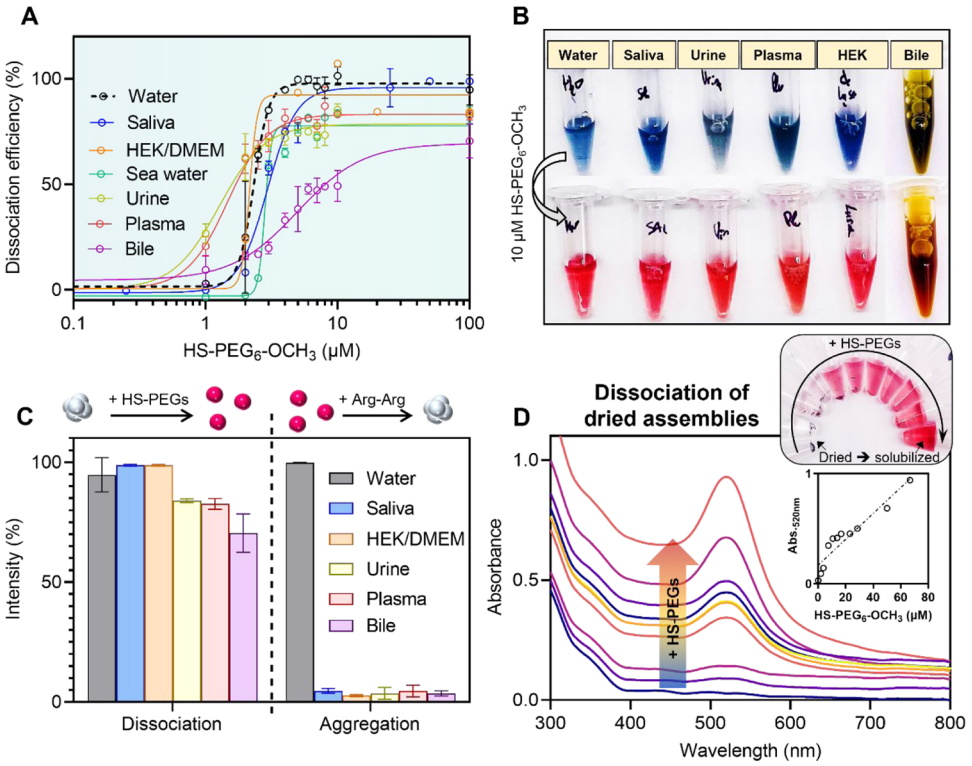

Figure 5. Dissociation of AuNP assemblies in complex matrices. (A) Dissociation efficiency of HS-PEG$_6$-OCH$_3$ added to Arg−Arg−AuNPs suspended in various media and (B) the corresponding pictures before and 20 min after the addition of 10 μM of HS-PEG$_6$-OCH$_3$. The complex medium was approximately 90% of the total volume except for the bile that was 20%. (C) Dissociation of Arg−Arg−AuNPs with HS-PEG$_6$-OCH$_3$ compared to that of the Arg−Arg-induced aggregation of AuNPs−citrate in various complex matrices. Note that HEK/DMEM corresponds to HEK 293 cell lysates coming from a suspension of 10^6 cells in Dulbecco's modified Eagle's media with 10% fetal bovine serum and 1% penicillin−streptomycin. (D) UV−vis spectra of the dried Arg−Arg−AuNP film after dissociation with an aqueous solution of HS-PEG$_6$-OCH$_3$ of various concentrations. Insets show the absorbance at 520 nm as a function of the concentration of HS-PEG$_6$-OCH$_3$ and the corresponding pictures.

assemblies (measured by MANTA) is inversely proportional to that of the HS-PEGx-OCH$_3$. This result was confirmed by UV−vis spectroscopy: HS-PEG$_x$-OCH$_3$ with a molecular weight of 20, 10, 5, and 2 kDa could only dissociate a maximum of 20, 35, 60, and 70% of the AuNP assemblies, respectively (Figure 4E−H). However, the 1 kDa HS-PEG$_x$-OCH$_3$ offered 80% dissociation; this value reached 100% for HS-PEG$_x$-OCH$_3$ with a molecular weight of 0.35 kDa or smaller (Figure 4I−K). These data illustrate that the dissociation efficiency of PEG is directly proportional to PEG size. Large HS-PEGs likely cannot reach the interfaces of the aggregated particles, while smaller HS-PEGs can. However, the concentration of HS-PEG$_x$-OCH$_3$ needed to initiate the dissociation was proportional to their size because the footprint of HS-PEGs is directly dependent on their size. Thus, larger HS-PEGs cover a larger surface on the AuNPs and less PEG molecules are needed to complete the coating. This nonexhaustive study reveals that the dissociation of AuNP assemblies can be directly modulated by tuning the PEG properties, and it is particularly interesting for the development of sensing strategies.

Advantages of the Dissociation Approach. Our dissociation approach possesses two major advantages compared to the conventional aggregation-based assay. First, it can operate across various complex samples, which is crucial for assay generalizability. Typically, background interferents differ across different sample matrices; thus, it is challenging to obtain an unambiguous colorimetric signal that is insensitive to the matrix composition—particularly for AuNP aggregation-based assays because the colloids can be unstable in these conditions or because endogenous molecules can prevent the aggregation. The dissociation of the AuNP assembly is very robust: it is unaffected by high ionic strength (>1 M NaCl) (Figure S8) or pH extremes (3 or 13) (Figure S9). Only compounds that can interact with the thiol group can interfere with the dissociation. As an example, dithiothreitol (DTT) quenching is presented in Figure S10. Thus, we next evaluated dissociation as a function of the sample type.

The dissociation of Arg−Arg−AuNP assemblies was investigated in the pooled plasma, pooled urine, pooled saliva, pooled bile, human embryonic kidney (HEK) 293 cell lysates in Dulbecco's modified Eagle's medium (DMEM), and even seawater. Importantly, the matrices by themselves could not dissociate the assemblies even after 3 h of incubation (Figure S11). This is particularly interesting because these complex environments usually produce dramatic background signals. For example, the dispersibility of AuNPs−citrate is strongly impacted when suspended in urine or seawater due to the high ionic strength (Figure S12). The dissociation of Arg−Arg−AuNPs in complex matrices was investigated with 10 μM of HS-PEG$_6$-OCH$_3$. Typically, concentrated Arg−Arg−AuNPs were suspended in the complex matrix and then HS-PEG$_6$-OCH$_3$ was added. The complex matrix represented at least 90% of the total volume. At least 80% of dissociation was obtained in all of the matrices including an unambiguous color change from blue to red (Figure 5A,B).

The redispersion of AuNP assemblies was then compared to the aggregation of dispersed AuNPs−citrate with the Arg−Arg peptide in complex media (Figure 5C). Even high concen-

https://doi.org/10.1021/acsami.2c17531
ACS Appl. Mater. Interfaces 2022, 14, 52553−52565

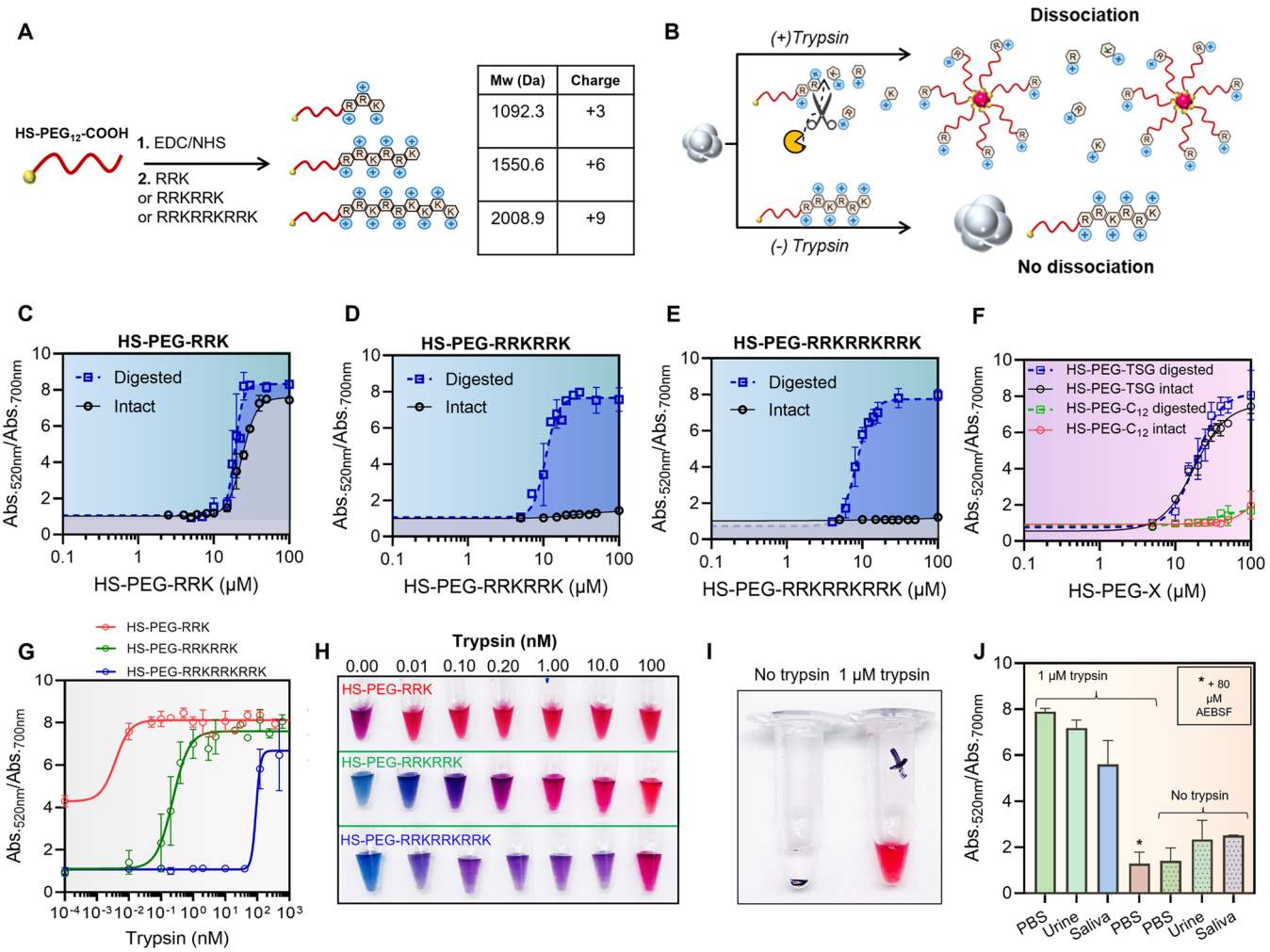

Figure 6. Trypsin sensing with HS-PEG−peptide conjugates. (A) Scheme of the synthesis of HS-PEG−peptide conjugates via EDC/NHS chemistry including the three main sequences investigated as well as the size and charge of the compounds. (B) Illustration of the sensing mechanism: the trypsin cleavage reduces the size and charge of the HS-PEG−peptide conjugate, which increases their capacity to dissociate the AuNP assemblies. Dissociation of Arg−Arg−AuNP assemblies with either (C) HS-PEG-RRK, (D) HS-PEG-RRKRRK, or (E) HS-PEG-RRKRRKRRK intact (black line) or digested by 1 μM of trypsin for 24 h at 37 °C (dashed blue line). (F) Dissociation of Arg−Arg−AuNP assemblies with HS-PEG-TSG and HS-PEG-C_{12} either intact or digested by trypsin. (G) Trypsin detection using the three different HS-PEG−peptide conjugates and (H) the corresponding pictures. (I) Picture of dried Arg−Arg−AuNP assemblies after the addition of 50 μL of HS-PEG-RRKRRK incubated or not with 1 μM of trypsin. (J) Comparison between the detection of 1 μM of trypsin spiked either in PBS or in urine as well as in PBS with 80 μM of AEBSF inhibitor.

trations of Arg−Arg (>200 μM) could not induce the AuNPs−citrate aggregation in biological fluids because of the numerous endogenous molecules/proteins that shield the electrostatic interactions between the peptide and the particles as well as the formation of a protein corona around the particles.[17] The matrix-insensitive feature of our dissociation design is explained by the fact that most of the biomolecules found in the complex samples (proteins, phospholipids, nucleotides, etc.) can only stick onto the gold surface via van der Waals forces, electrostatic or hydrophobic interactions, or hydrogen bonds.[17,36] Thus, the grafting of HS-PEGs is favored because the Au−S bond energy is approximately 10-fold higher than the average hydrogen bond.[37] Also, PEGs are commonly used to prevent the nonspecific adsorption of proteins on AuNPs, and thus the HS-PEGs do not interact much with the interferents; they remain free to bind to the particles.

The second advantage of our dissociation approach is that the assemblies did not just remain aggregated—they also precipitated, thus increasing the color change between the dissociated and aggregated systems. As an example, Figure S13 shows that Arg−Arg−AuNPs suspended in saliva after 2 h tend to precipitate, thus leading to a loss of blue color in the suspension, while the dissociated particles remain bright red. Interestingly, even if precipitated, the assemblies can still be dissociated with 10 μM of HS-PEG_6-OCH_3.

Remarkably, the HS-PEGs could even solubilize dried films of Arg−Arg−AuNPs (Figure 5D). Briefly, 50 μL of aqueous solution containing different concentrations of HS-PEGs, ranging from 0 to 70 μM, was added to the dried particles, and 20 min later, the UV−vis spectrum of the solution was recorded. In the absence of HS-PEGs, no LSPR band of the particles was observed as no particles detached spontaneously and the solution remained clear. However, in the presence of HS-PEGs, the plasmonic band of the particles was observed proportionally to the HS-PEG concentration without the need for sonication. The HS-PEGs led to the spontaneous and progressive detachment of the AuNPs from the surface and thus a color change (Figure 5D, inset). The solubilization of the AuNPs could thus be quantified using only the absorbance at 520 nm in the solution as the LSPR band intensity was linearly

https://doi.org/10.1021/acsami.2c17531
ACS Appl. Mater. Interfaces 2022, 14, 52553−52565

proportional to the HS-PEG concentration. This approach did not work on AuNPs−citrate as they degraded during the drying process—the dipeptide is a crucial additive. Finally, the solubilization of dried Arg−Arg−AuNPs was possible even in biofluids such as saliva, plasma, urine, or cell lysates (see the Supporting Information Figure S14).

Thus, our dissociation strategy affords two advantages versus traditional aggregation-based assays: it is insensitive to the composition of the operating medium and the gap of colorimetric signals between dissociated and nondissociated samples is unambiguous and increases over time, thus enhancing the naked eye identification.

Protease Detection. The charge and size of the HS-PEGs modulate their capacity to dissociate the AuNP assemblies, and thus we designed a strategy to detect proteases in biological fluids. Trypsin was chosen as a model protease because it possesses a high catalytic efficiency and easily cleaves peptide sequences after arginine or lysine.[38] Trypsin is a biomarker of pancreatic cancer and can be found in micromolar concentrations in blood or urine.[39]

Peptides containing the motif Arg−Arg−Lys (RRK) were thus conjugated to a thiolated PEG capped with a carboxyl group (HS-PEG_{12}-COOH, Mw = 634 Da) via EDC/NHS cross-linking reaction. Three peptides based on the motif RRK were investigated, and the number of RRK repetitions varied from 1 to 3 to increase the mass and charge of the resulting HS-PEG−peptide conjugate (Figure 6A).

From concentrations of 10 μM, HS-PEG_{12}-COOH is capable of dissociating 100% of the assemblies (Figure S15). However, the conjugation of the peptides to the HS-PEG_{12}-COOH was expected to decrease its capacity to dissociate the assemblies as it increases its size and charge. In this context, the addition of the HS-PEG−peptide conjugates to AuNP assemblies could not generate a colorimetric signal. However, in the presence of trypsin, the proteolytic cleavage could progressively remove the amino acid residues from the conjugate, thus reducing its size and charge that would restore the dissociation capacity. A colorimetric signal, proportional to the trypsin activity, could thus be observed (Figure 6B).

The HS-PEG−peptide conjugates were synthesized and titrated to Arg−Arg−AuNP assemblies to evaluate the quenching of their dissociation capacity. EDC/NHS cross-linking between HS-PEG-COOH and RRKRRK or RRKRRKRRK led to a total quenching of the dissociation capacity of HS-PEG_{12}-COOH even at high concentrations (>100 μM) (Figure 6D,F), while the conjugation of RRK only reduced it slightly (Figure 6E). In the absence of EDC/NHS, no cross-linking could occur and the dissociation capacity of HS-PEG_{12}-COOH was not affected (Figure S16).

Subsequently, the three conjugates were digested with trypsin (10 μM, 37 °C, 24 h) and titrated into the AuNP assemblies again. Interestingly, the dissociation capacity of HS-PEG-RRKRRK and HS-PEG-RRKRRKRRK was restored; HS-PEG-RRK was also enhanced because cleavage by trypsin reduced the size and the positive charge of the conjugate (Figure 6C−E). A minimum of two repetitions of the motif RRK is thus necessary to ensure a total quenching of the dissociation capacity of the HS-PEG_{12}-COOH. This can later be completely restored with the proteolytic cleavage. Only one repetition of RRK leads to a very narrow window of detection between the intact and digested HS-PEG−peptide. In addition to conferring a higher positive charge, the RRKRRK and RRKRRKRRK peptides could conjugate multiple HS-PEGs per peptide due to the presence of lysine residues that, in turn, lead to an even bigger construct. Matrix-assisted laser desorption/ionization (MALDI) was used to characterize the HS-PEG-RRKRRK conjugate (Figure S17), and a mixture of single and multiple conjugations of HS-PEG per peptide was observed.

Control experiments were then conducted with alternative nontrypsin-cleavable molecules: the peptide TSG and the bis-amine C_{12}. The resulting conjugates (HS-PEG-TSG and HS-PEG-C_{12}) were then titrated to Arg−Arg−AuNP assemblies before and after digestion with trypsin, similarly to what was described previously. The dissociation capacity of HS-PEG-TSG was similar to that of HS-PEG_{12}-COOH because TSG is a short peptide and lacks a positive charge. It is not impacted by the digestion of trypsin. On the other hand, the conjugation of C_{12} led to total quenching of the dissociation capacity that could not be restored with trypsin digestion. This is because C_{12}, like RRKRRK and RRKRRKRRK, contains more than one free amine and can thus be conjugated to multiple HS-PEG molecules. This makes the conjugate too bulky to dissociate the AuNPs. However, unlike RRKRRK and RRKRRKRRK, C_{12} does not have any cleavable site for trypsin and thus the trypsin digestion has no effect on the dissociation capacity (Figure 6F).

HS-PEG-RRK, HS-PEG-RRKRRKRRK, and HS-PEG-RRKRRKRRK were then used to detect different concentrations of trypsin (Figure 6G). Briefly, the HS-PEG−peptide conjugates were incubated with various concentrations of trypsin in PBS (pH = 7.4) for 2 h at 37 °C, and then Arg−Arg−AuNP assemblies were added; the color change of the suspension was analyzed 10 min later. An LOD of <100 pM was observed for HS-PEG-RRK and HS-PEG-RRKRRK, while an LOD of 100 nM was obtained for HS-PEG-RRKRRKRRK. This is because more intense proteolytic activity is required to release HS-PEG fragments from HS-PEG-RRKRRKRRK that can dissociate the assemblies.

As the quenching of HS-PEG-RRK was not complete, a high background signal was observed (50% of dissociation was obtained even in the absence of trypsin) (Figure 6G). Therefore, the color of the samples in the absence of trypsin was purple, but it remained blue for HS-PEG-RRKRRK and HS-PEG-RRKRRKRRK. Figure 6H shows the pictures of the samples for the detection of various concentrations of trypsin. HS-PEG-RRKRRK affords the best combination of sensitivity and LOD among the three peptide sequences compared here. The results that we obtained with repeated RRK motifs agree well with what has been reported for the fluorescence detection of trypsin with similar sequences.[40] Importantly, the detection of trypsin with HS-PEG-RRKRRK could also be performed on the dried film of Arg−Arg−AuNP assemblies: 30 min after the addition of 50 μL of HS-PEG-RRKRRK incubated with 1 μM of trypsin, the AuNPs detached from the surface and the solution became red (Figure 6I). In the absence of trypsin, the particles remained attached to the surface. This shows that the solubilization of dried AuNPs can be used for protease detection with the generation of a strong unambiguous colorimetric signal for samples containing the analyte, thus facilitating simple detection by eyes.

Next, pooled urine and saliva were spiked with 1 μM of trypsin and incubated with HS-PEG-RRKRRK for 2 h; Arg−Arg−AuNP were added as readout elements. A colorimetric signal similar to what was obtained in buffer was observed in the presence of trypsin. Interestingly, no signal was generated in the absence of trypsin (Figure 6J). Even more interesting, the limit of detection of trypsin in saliva was similar to that in buffer (ca.

https://doi.org/10.1021/acsami.2c17531
ACS Appl. Mater. Interfaces 2022, 14, 52553−52565

<100 pM) (Figure S18). This shows that the dissociation strategy using the HS-PEG−peptide as a substrate can detect proteases in pure biological fluids without the need for extreme dilution of the sample or separation procedures. It is worth mentioning that the detection of trypsin in saliva could also be performed with the dried AuNPs.

Finally, we used a known trypsin-competitive inhibitor, 4-(2-aminoethyl)benzenesulfonyl fluoride hydrochloride (AEBSF),[41] to study the inhibition of trypsin proteolytic activity with the HS-PEG-RRKRRK substrate. Briefly, HS-PEG-RRKRRK was first mixed with various concentrations of AEBSF for 30 min and then incubated with 1 μM of trypsin. HS-PEG-RRKRRK incubated with 1 μM of trypsin initially mixed with 80 μM of AEBSF led to no dissociation of the AuNPs, thus indicating trypsin inhibition by AEBSF (Figure 6J). The results confirm that the restoration of the dissociation capacity of the HS-PEG−peptide conjugates in the presence of trypsin is due to trypsin's enzymatic activity (see Supporting Information Figure S19 for the typical inhibitor titration curve and the potency of the AEBSF inhibitor). Of note, AEBSF alone does not impact the dispersion of the AuNP assemblies. This inhibition study shows that our sensing strategy can rapidly screen therapeutic agents.

CONCLUSIONS

In summary, the dissociation of AuNP assemblies with HS-PEG molecules was studied and exploited to build matrix-insensitive sensors. Robust assemblies of AuNPs−citrate were formed using a di-arginine additive (Arg−Arg). The efficient electrostatic interactions between the citrate and the arginine led to compact assemblies of the particles, thus provoking a strong modification of their optical properties. However, the presence of peptides protected the AuNPs from degradation. Surprisingly, the addition of HS-PEGs could dissociate the assemblies with a total recovery of the initial optical properties. The mechanism was fully characterized by TEM, MANTA, UV−vis, and FTIR spectroscopies. The HS-PEGs can progressively graft onto the AuNP surface and remove the citrate/arginine layers. As the hydrophilic PEG layer surrounds the AuNPs, the particles progressively detach from the bulky assemblies and become water-dispersible. Importantly, only a minimum amount of HS-PEGs is needed to cover all of the gold surfaces (~4 HS-PEG$_6$-OCH$_3$/nm^2). We have thus shown that the dissociation capacity of HS-PEGs is modulated by their size and charge. HS-PEG-OCH$_3$ with a molecular weight of 1000 Da or less could dissociate 80% or more. Remarkably, the dissociation of the assemblies was matrix-insensitive and produced an unambiguous color change in plasma, saliva, urine, bile, cell lysates, or even seawater. Moreover, we found that the generation of the colorimetric signal could be improved using a dried film of AuNP assemblies. The presence of HS-PEGs leads to the detachment of AuNPs from the surface as it solubilizes them. The color of the suspension becomes then red, and its intensity is proportional to the amount of HS-PEGs. In the absence of this later, the color of the solution is clear. This strategy allows an unambiguous distinction with the naked eyes between samples that have or no HS-PEGs. We thus designed a sensing strategy based on HS-PEG−peptide probes and AuNP assemblies as a signal readout for protease sensing in complex media. Trypsin was chosen as the model protease, and the peptide-containing repetition of the motif RRK was conjugated to HS-PEGs. The optimized conjugate, HS-PEG-RRKRRK, allowed the visual detection of trypsin with a picomolar limit of detection. Detection could be performed simply in pooled urine or saliva spiked with trypsin. To the best of our knowledge, this is the first time that HS-PEG molecules have been used to dissociate AuNP assemblies or to solubilize dried AuNPs and combined with peptides for protease detection. This innovative approach could benefit protease detection across various complex environments. The approach could be adapted to any protease as long as a peptide substrate can be conjugated to HS-PEGs and the dissociation capacity of the resulting conjugate can only be restored by the proteolytic activity.

EXPERIMENTAL SECTION

AuNP Synthesis. Citrate-stabilized AuNPs (~20 nm) were prepared using the Turkevich method by rapidly injecting an aqueous solution of sodium citrate tribasic dihydrate (150 mg, 5 mL) into an aqueous solution of $HAuCl_4 \cdot 3H_2O$ (45 mg, 300 mL) under boiling conditions and vigorous stirring. The reaction mixture was left boiling while stirring for another 15 min and then cooled down to room temperature. The deep red dispersion was then purified by applying one round of centrifugation at 18,000g for 30 min, and the pink supernatant was discarded. The resulting pellet of AuNPs−citrate was redispersed in deionized water by sonication and stored at ambient conditions.

AuNP Assembly and Dissociation. Typically, 1 mL of AuNPs−citrate at OD = 1.5 was mixed with 50 μL of Arg−Arg (100 μM) to provoke the AuNP assembly. The color of the suspensions rapidly changed from red to blue. The assembled AuNPs (Arg−Arg−AuNPs) were stable over time when stored at 4 °C and could be used for dissociation even a month after their assembly. Dissociation: stock solutions of the different HS-PEGs with concentrations ranging from 10 μM to 1 mM were prepared. Specific volumes of each solution were added to a 96-well plate to reach the desired final HS-PEG concentration, and then 100 μL of Arg−Arg−AuNPs was added. For complex matrix experiments, the Arg−Arg−AuNPs were first concentrated 10 times by centrifugation and then dispersed in complex media (seawater, pooled human saliva, plasma, urine, bile, or HEK cell lysates) that represented thus 90% of the total volume except for bile, which was only 20%. Quickly after the addition of AuNPs, the dissociation of the assembly was monitored and the ratio of the absorbances at 520 and 700 nm was recorded over time. The percentage of dissociation is described as follows

$$\%\ \text{of dissociation} = \frac{\left(\frac{\text{Abs520 nm}}{\text{Abs700 nm}}\right)_{\text{AuNPs-S-PEGs}} - \left(\frac{\text{Abs520 nm}}{\text{Abs700 nm}}\right)_{\text{Arg-Arg-AuNPs}}}{\left(\frac{\text{Abs520 nm}}{\text{Abs700 nm}}\right)_{\text{AuNPs-citrate}} - \left(\frac{\text{Abs520 nm}}{\text{Abs700 nm}}\right)_{\text{Arg-Arg-AuNPs}}}$$

where $\left(\frac{\text{Abs520 nm}}{\text{Abs700 nm}}\right)_{\text{AuNPs-S-PEGs}}$ is the ratio of the absorbance after dissociation with HS-PEGs, $\left(\frac{\text{Abs520 nm}}{\text{Abs700 nm}}\right)_{\text{AuNPs-citrate}}$ is the ratio of the absorbance of the initial citrate-capped AuNPs, and $\left(\frac{\text{Abs520 nm}}{\text{Abs700 nm}}\right)_{\text{Arg-Arg-AuNPs}}$ is the ratio of the arginine-induced assembly of AuNPs.

Drying and Solubilization of the AuNP Assemblies. First, 1 mL of AuNPs−citrate was concentrated 5 times by centrifugation (18,000g for 18 min). Then, the assembly was provoked by adding 25 μL of Arg−Arg (100 μM) to the resulting 200 μL of concentrated AuNPs-−citrate. Finally, 10 μL of the concentrated Arg−Arg−AuNPs was added to an Eppendorf and dried at 40 °C overnight. The solubilization of the dried assemblies with HS-PEGs was performed similarly to the dissociation of the assemblies. It is worth noting that vigorously shaking the Eppendorf could be required.

Peptide Synthesis. Peptides Arg−Arg (RR), Arg−Arg−Arg−Arg−Arg (RRRRR), Arg−Gly−Gly−Gly−Arg (RGGGR), and Tyr−Ser−Gly (TSG) were synthesized using an automated Eclipse peptide synthesizer (AAPPTec, Louisville, KY) through standard solid-phase Fmoc synthesis on Rink-amide resin. Peptides were lyophilized in a

https://doi.org/10.1021/acsami.2c17531
ACS Appl. Mater. Interfaces 2022, 14, 52553−52565

FreeZone Plus 2.5 freeze dry system (Labconco Corp., Kansas, MO). Peptide purification used a Shimadzu LC-40 HPLC system equipped with an LC-40D solvent delivery module, a photodiode array detector SPD-M40, and a degassing unit DGU-403. The crude sample was dissolved in an acetonitrile/H_2O mixture (1:1, v/v) with an injection volume of 2 mL. This was applied on a Zorbax 300 BS, C18 column (5 μm, 9.4 × 250 mm) from Agilent (Santa Clara, CA) and eluted at a flow rate of 1.5 mL/min over a 40 min linear gradient from 10 to 95% of acetonitrile in water (with 0.05% TFA, HPLC grade). Preparative injections were monitored at an absorbance of 190, 220, and 254 nm. Fractions containing the pure peptide as confirmed by electrospray ionization mass spectroscopy were lyophilized and aliquoted (see below). All peptides were purified by HPLC to reach a purity of at least 90%. Peptide synthesis was confirmed by electrospray ionization mass spectrometry (ESI-MS, positive ion mode) via the Micromass Quattro Ultima mass spectrometer in the Molecular MS Facility (MMSF). ESI-MS samples were prepared in a MeOH/H_2O mixture (1:1, v/v).

HS-PEG−Peptide Conjugate Synthesis. Typically, 1 mL of HS-PEG_{12}-COOH (HS-$(CH_2CH_2O)_{12}$-CH_2CH_2COOH, 634 Da, 1 mM) dissolved in MES buffer (10 mM, pH = 5.5) was activated via the addition of 100 μL of EDC (50 mM, MES) and 40 μL of NHS (500 mM, MES). The reaction was stirred at room temperature for 1 h. After 1 h, 1 mL of peptide (or NH_2-molecule) (1 mM) dissolved in PBS (100 mM, pH = 7.4) was added to the activated HS-PEG_{12}-COOH. The reaction was stirred for 4 h at room temperature and then stored at 4 °C.

Trypsin Incubation. Typically, 5 μL of the PEG−peptide conjugate (0.44 mM) was added to 5 μL of PBS 1×. Subsequently, 2 μL of trypsin of various concentrations was added and the resulting solution was incubated at 37.5 °C for 2 h. At the end of the incubation, 100 μL of aggregated AuNPs (Arg−Arg−AuNPs) was added, and a color change proportional to the trypsin concentration was observed. UV−vis spectra were recorded 30 min later.

Trypsin Inhibition Study. Aqueous AEBSF inhibitor solution (20 mM) was prepared, and a specific volume was mixed with 1 μM of trypsin to reach the desired final AEBSF concentration. The resulting mixture was stirred gently at room temperature for 30 min. Subsequently, the specific volume of HS-PEG-RRKRRK was added to reach a final concentration of 200 μM and the solution was incubated at 37.5 °C for 2 h. Finally, 100 μL of Arg−Arg−AuNPs (20 nm) was added, and the UV−vis spectrum was recorded 10 min later.

UV−Vis Spectroscopy. The optical absorption measurements were collected using a hybrid multimode microplate reader (Synergy H1 model, BioTek Instruments, Inc.) in a 96-well plate. The dissociation of assembly was characterized by measuring the ratio of the absorbance at 520 or 530 and 700 or 820 nm for 20 or 40 nm NPs, respectively.

ATR-FTIR Spectroscopy. ATR-FTIR spectra were recorded with a Nicolet iS50 FTIR spectrometer with a DLaTGS detector by natural drying of 1 μL of AuNP suspensions. Typically, 1 mL of AuNPs (2 nM) was first cleaned from unbound molecules via four cycles of centrifugation (18,000g during 18 min) and resuspended in 40 μL of pure water. The final concentration was then approximately 50 nM.

Transmission Electron Microscopy (TEM). Transmission electron microscopy (TEM) images of the Au colloids were acquired using a JEOL 1200 EX II operating at 80 kV. The TEM grids were prepared by the natural drying of 2 μL of 2 nM AuNPs.

Multispectral Advanced Nanoparticle Tracking Analysis (MANTA). The multispectral advanced nanoparticle tracking analysis (MANTA) is a technique that builds images from the particles' light scattering via three lasers of different wavelengths (e.g., blue, green, and red); the wavelength of scattering depends on nanoparticle size. Thus, small particles (<100 nm) appear blue, while larger particles appear greener or redder. MANTA uses these images to count the nanoparticles and calculate their size based on Brownian motion. MANTA was performed with the ViewSizer 3000 (Horiba Scientific). The temperature was set to 25 °C during the measurement. Automated noise analysis determines the optimal wavelength for representing each nanoparticle. Here, 8-bit composite videos were generated, and 10 videos were used per analysis (300 frames for seconds). A quartz cuvette with a minimum volume of 1 mL was used for the measurement, and the AuNP concentration was set up at 0.04 nM.

Cell Culture. A human embryonic kidney cell line (HEK 293T) was used for this work. The cells were cultured in Dulbecco's modified Eagle's medium (DMEM) with 10% fetal bovine serum (FBS) and 1% penicillin−streptomycin. The cells were incubated at 37 °C, 5% CO_2, and the media was replaced every 2 days. Cells were passaged at a 75−80% confluency using trypsin-EDTA (0.25%); 1,000,000 HEK 293T cell samples were harvested by detaching the cells with trypsin-EDTA (0.25%), centrifugation at 700 rcf for 5 min, and resuspending in PBS for further experiments. The cell lysate was prepared by mechanical disruption via freeze−thaw cycles.

■ ASSOCIATED CONTENT

Supporting Information

The Supporting Information is available free of charge at https://pubs.acs.org/doi/10.1021/acsami.2c17531.

Materials, instrumentations, methods, video of AuNP dissociation, TEM images, stability over time, dissociation kinetics, dissociation in NaCl, dissociation at different pH values, and dissociation with DTT, 40 nm NP study (PDF)

A video of the dissociation of the AuNP assemblies (MP4)

■ AUTHOR INFORMATION

Corresponding Author

Jesse V. Jokerst − *Department of NanoEngineering, University of California, San Diego, La Jolla, California 92093, United States; Materials Science and Engineering Program and Department of Radiology, University of California, San Diego, La Jolla, California 92093, United States;* orcid.org/0000-0003-2829-6408; Email: jjokerst@ucsd.edu

Authors

Maurice Retout − *Department of NanoEngineering, University of California, San Diego, La Jolla, California 92093, United States*

Zhicheng Jin − *Department of NanoEngineering, University of California, San Diego, La Jolla, California 92093, United States;* orcid.org/0000-0001-6072-7533

Jason Tsujimoto − *Department of Bioengineering, University of California, San Diego, La Jolla, California 92093, United States*

Yash Mantri − *Department of Bioengineering, University of California, San Diego, La Jolla, California 92093, United States;* orcid.org/0000-0002-6689-2158

Raina Borum − *Department of NanoEngineering, University of California, San Diego, La Jolla, California 92093, United States;* orcid.org/0000-0003-4265-3109

Matthew N. Creyer − *Department of NanoEngineering, University of California, San Diego, La Jolla, California 92093, United States;* orcid.org/0000-0003-1213-8245

Wonjun Yim − *Materials Science and Engineering Program, University of California, San Diego, La Jolla, California 92093, United States;* orcid.org/0000-0002-0242-7898

Tengyu He − *Materials Science and Engineering Program, University of California, San Diego, La Jolla, California 92093, United States;* orcid.org/0000-0002-6767-4849

Yu-Ci Chang − *Materials Science and Engineering Program, University of California, San Diego, La Jolla, California 92093, United States;* orcid.org/0000-0001-6997-9884

Complete contact information is available at:

https://pubs.acs.org/10.1021/acsami.2c17531

Notes

The authors declare no competing financial interest.

■ ACKNOWLEDGMENTS

The authors thank the National Institutes of Health (R01 DE031114; R21 AG065776; R21 AI157957; and S10 OD023555-01A1) for financial support. This work was supported, in part, by the National Science Foundation Graduate Research Fellowship Program under Grant No. DGE-1650112. The electron microscopy work was performed, in part, at the San Diego Nanotechnology Infrastructure (SDNI) of the University of California San Diego, a member of the National Nanotechnology Coordinated Infrastructure (NNCI), which was supported by the National Science Foundation (Grant ECCS-1542148). M.R. thanks the Wallonie-Bruxelles International Foundation. This work used equipment purchased supported by the UC San Diego Materials Research Science and Engineering Center (UCSD MRSEC), supported by the National Science Foundation (Grant DMR-2011924). M.N.C. and R.M.B. acknowledge training fellowship support from the NIH via T32 CA153915.

■ REFERENCES

(1) Liu, X.; Atwater, M.; Wang, J.; Huo, Q. Extinction Coefficient of Gold Nanoparticles with Different Sizes and Different Capping Ligands. *Colloids Surf., B* **2007**, *58*, 3−7.

(2) Pramanik, A.; Gao, Y.; Patibandla, S.; Mitra, D.; McCandless, M. G.; Fassero, L. A.; Gates, K.; Tandon, R.; Chandra Ray, P. The Rapid Diagnosis and Effective Inhibition of Coronavirus Using Spike Antibody Attached Gold Nanoparticles. *Nanoscale Adv.* **2021**, *3*, 1588−1596.

(3) Saha, K.; Agasti, S. S.; Kim, C.; Li, X.; Rotello, V. M. Gold Nanoparticles in Chemical and Biological Sensing. *Chem. Rev.* **2012**, *112*, 2739−2779.

(4) Gosselin, B.; Retout, M.; Dutour, R.; Troian-gautier, L.; Bevernaegie, R.; Herens, S.; Lefevre, P.; Denis, O.; Bruylants, G.; Jabin, I. Ultrastable Silver Nanoparticles for Rapid Serology Detection of Anti-SARS-CoV-2 Immunoglobulins G. *Anal. Chem.* **2022**, *94*, 7383−7390.

(5) Kelly, K. L.; Coronado, E.; Zhao, L. L.; Schatz, G. C. The Optical Properties of Metal Nanoparticles: The Influence of Size, Shape, and Dielectric Environment. *J. Phys. Chem. B* **2003**, *107*, 668−677.

(6) Jain, P. K.; Huang, X.; El-Sayed, I. H.; El-Sayed, M. A. Review of Some Interesting Surface Plasmon Resonance-Enhanced Properties of Noble Metal Nanoparticles and Their Applications to Biosystems. *Plasmonics* **2007**, *2*, 107−118.

(7) Kimling, J.; Maier, M.; Okenve, B.; Kotaidis, V.; Ballot, H.; Plech, A. Turkevich Method for Gold Nanoparticle Synthesis Revisited. *J. Phys. Chem. B* **2006**, *110*, 15700−15707.

(8) Jin, Z.; Mantri, Y.; Retout, M.; Cheng, Y.; Zhou, J.; Jorns, A.; Fajtova, P.; Yim, W.; Moore, C.; Xu, M.; Creyer, M.; Borum, R.; Zhou, J.; Wu, Z.; He, T.; Penny, W.; O'Donoghue, A.; Jokerst, J. A Charge-Switchable Zwitterionic Peptide for Rapid Detection of SARS-CoV-2 Main Protease. *Angew. Chem., Int. Ed.* **2022**, *61*, No. e202112995.

(9) Sun, J.; Lu, Y.; He, L.; Pang, J.; Yang, F.; Liu, Y. Colorimetric Sensor Array Based on Gold Nanoparticles: Design Principles and Recent Advances. *TrAC, Trends Anal. Chem.* **2020**, *122*, No. 115754.

(10) Hu, T.; Lu, S.; Chen, C.; Sun, J.; Yang, X. Colorimetric Sandwich Immunosensor for Aβ(1-42) Based on Dual Antibody-Modified Gold Nanoparticles. *Sens. Actuators, B* **2017**, *243*, 792−799.

(11) Retout, M.; Valkenier, H.; Triffaux, E.; Doneux, T.; Bartik, K.; Bruylants, G. Rapid and Selective Detection of Proteins by Dual Trapping Using Gold Nanoparticles Functionalized with Peptide Aptamers. *ACS Sens.* **2016**, *1*, 929−933.

(12) Vilela, D.; González, M. C.; Escarpa, A. Sensing Colorimetric Approaches Based on Gold and Silver Nanoparticles Aggregation: Chemical Creativity behind the Assay. A Review. *Anal. Chim. Acta* **2012**, *751*, 24−43.

(13) He, H.; Dai, J.; Duan, Z.; Zheng, B.; Meng, Y.; Guo, Y.; Xiao, D. Unusual Sequence Length-Dependent Gold Nanoparticles Aggregation of the SsDNA Sticky End and Its Application for Enzyme-Free and Signal Amplified Colorimetric DNA Detection. *Sci. Rep.* **2016**, *6*, No. 27711.

(14) Lin, S.-Y.; Wu, S.-H.; Chen, C. A Simple Strategy for Prompt Visual Sensing by Gold Nanoparticles: General Applications of Interparticle Hydrogen Bonds. *Angew. Chem.* **2006**, *118*, 5070−5073.

(15) Hamaker, H. C. The London-van Der Waals Attraction between Spherical Particles. *Physica* **1937**, *4*, 1058−1072.

(16) Retout, M.; Mantri, Y.; Jin, Z.; Zhou, J.; Noël, G.; Donovan, B.; Yim, W.; Jokerst, Jv. Peptide-Induced Fractal Assembly of Silver Nanoparticles for Visual Detection of Disease Biomarkers. *ACS Nano* **2022**, *16*, 6165−6175.

(17) Charbgoo, F.; Nejabat, M.; Abnous, K.; Soltani, F.; Taghdisi, S. M.; Alibolandi, M.; Thomas Shier, W.; Steele, T. W. J.; Ramezani, M. Gold Nanoparticle Should Understand Protein Corona for Being a Clinical Nanomaterial. *J. Controlled Release* **2018**, *272*, 39−53.

(18) Liang, X.; Wei, H.; Cui, Z.; Deng, J.; Zhang, Z.; You, X.; Zhang, X. E. Colorimetric Detection of Melamine in Complex Matrices Based on Cysteamine-Modified Gold Nanoparticles. *Analyst* **2011**, *136*, 179−183.

(19) Retout, M.; Gosselin, B.; Mattiuzzi, A.; Ternad, I.; Jabin, I.; Bruylants, G. Peptide-Conjugated Silver Nanoparticles for the Colorimetric Detection of the Oncoprotein Mdm2 in Human Serum. *Chempluschem* **2022**, *87*, No. e202100450.

(20) Lin, L.; Tseng, W.-L.; Wu, V. C. H.; Quintela, I. A.; de Los Reyes, B. G.; Lin, C.-S. Simultaneous Colorimetric Detection of a Variety of *Salmonella* Spp. in Food and Environmental Samples by Optical Biosensing Using Oligonucleotide-Gold Nanoparticles. *Front. Microbiol.* **2019**, No. 1138.

(21) Derjaguin, V.The Derjaguin-Landau-Verwey- Overbeek (DLVO) Theory Stability of Lyophobic Colloids. In *Surface Forces*; Springer: Boston, MA, 1987; pp 293−294.

(22) Mani, E.; Lechner, W.; Kegel, W. K.; Bolhuis, P. G. Equilibrium and Non-Equilibrium Cluster Phases in Colloids with Competing Interactions. *Soft Matter* **2014**, *10*, 4479−4486.

(23) Liu, D.; Chen, W.; Sun, K.; Deng, K.; Zhang, W.; Wang, Z.; Jiang, X. Resettable, Multi-Readout Logic Gates Based on Controllably Reversible Aggregation of Gold Nanoparticles. *Angew. Chem.* **2011**, *123*, 4189−4193.

(24) He, H.; Feng, M.; Chen, Q.; Zhang, X.; Zhan, H. Light-Induced Reversible Self-Assembly of Gold Nanoparticles Surface-Immobilized with Coumarin Ligands. *Angew. Chem.* **2016**, *128*, 948−952.

(25) Hazarika, P.; Ceyhan, B.; Niemeyer, C. M. Reversible Switching of DNA-Gold Nanoparticle Aggregation. *Angew. Chem.* **2004**, *116*, 6631−6633.

(26) Trantakis, I. A.; Bolisetty, S.; Mezzenga, R.; Sturla, S. J. Reversible Aggregation of DNA-Decorated Gold Nanoparticles Controlled by Molecular Recognition. *Langmuir* **2013**, *29*, 10824−10830.

(27) Retout, M.; Ivan, Jabin.; Bruylants, G. Synthesis of Ultra-Stable and Bioconjugable Ag, Au and Bimetallic Ag_Au Nanoparticles Coated with Calix[4]Arenes. *ACS Omega* **2021**, *6*, 19675−19684.

(28) Retout, M.; Cornelio, B.; Bruylants, G.; Jabin, I. Bifunctional Calix[4]Arene-Coated Gold Nanoparticles for Orthogonal Conjugation. *Langmuir* **2022**, *38*, 9301−9309.

(29) Moore, C.; Wing, R.; Pham, T.; Jokerst, Jv. Multispectral Nanoparticle Tracking Analysis for the Real-Time and Label-Free Characterization of Amyloid-β Self-Assembly in Vitro. *Anal. Chem.* **2020**, *92*, 11590−11599.

(30) Retout, M.; Blond, P.; Jabin, I.; Bruylants, G. Ultrastable PEGylated Calixarene-Coated Gold Nanoparticles with a Tunable Bioconjugation Density for Biosensing Applications. *Bioconjugate Chem.* **2021**, *32*, 290−300.

(31) Smith, M. C.; Crist, R. M.; Clogston, J. D.; Mcneil, S. E. Quantitative Analysis of PEG-Functionalized Colloidal Gold Nanoparticles Using Charged Aerosol Detection. *Anal. Bioanal. Chem.* **2015**, *407*, 3705−3716.
(32) Jokerst, J. V.; Lobovkina, T.; Zare, R. N.; Gambhir, S. S. Nanoparticle PEGylation for Imaging and Therapy. *Nanomedicine* **2011**, *6*, 715−728.
(33) Retout, M.; Brunetti, E.; Valkenier, H.; Bruylants, G. Limits of Thiol Chemistry Revealed by Quantitative Analysis of Mixed Layers of Thiolated-PEG Ligands Grafted onto Gold Nanoparticles. *J. Colloid Interface Sci.* **2019**, *557*, 807−815.
(34) Ghann, W.; Harris, T.; Kabir, D.; Kang, H.; Jiru, M.; Rahman, M. M.; Ali, M. M.; Uddin, J. Lipoic Acid Decorated Gold Nanoparticles and Their Application in the Detection of Lead Ions. *J. Nanomed. Nanotechnol.* **2019**, *10*, 539.
(35) Fracasso, D.; Kumar, S.; Rudolf, P.; Chiechi, R. C. Self-Assembled Monolayers of Terminal Acetylenes as Replacements for Thiols in Bottom-up Tunneling Junctions. *RSC Adv.* **2014**, *4*, 56026−56030.
(36) Zhdanov, V. P. Nanoparticles without and with Protein Corona: Van Der Waals and Hydration Interaction. *J. Biol. Phys.* **2019**, *45*, 307−316.
(37) de La Llave, E.; Ricci, A.; Calvo, E. J.; Scherlis, D. A. Binding between Carbon and the Au(111) Surface and What Makes It Different from the S-Au(111) Bond. *J. Phys. Chem. C* **2008**, *112*, 17611−17617.
(38) Yang, J.; Gao, Z.; Ren, X.; Sheng, J.; Xu, P.; Chang, C.; Fu, Y. DeepDigest: Prediction of Protein Proteolytic Digestion with Deep Learning. *Anal. Chem.* **2021**, *93*, 6094−6103.
(39) Guo, H.; Song, S.; Dai, T.; Sun, K.; Zhou, G.; Li, M.; Mann, S.; Dou, H. Near-Infrared Fluorescent and Magnetic Resonance Dual-Imaging Coacervate Nanoprobes for Trypsin Mapping and Targeted Payload Delivery of Malignant Tumors. *ACS Appl. Mater. Interfaces* **2020**, *12*, 17302−17313.
(40) Moore, C.; Borum, R. M.; Mantri, Y.; Xu, M.; Fajtová, P.; O'Donoghue, A. J.; Jokerst, Jv. Activatable Carbocyanine Dimers for Photoacoustic and Fluorescent Detection of Protease Activity. *ACS Sens.* **2021**, *6*, 2356−2365.
(41) de Souza Nascimento, A. M.; de Oliveira Segundo, V. H.; Felipe Camelo Aguiar, A. J.; Piuvezam, G.; Souza Passos, T.; Florentino da Silva Chaves Damasceno, K. S. F. da S.; de Araújo Morais, A. H.Antibacterial Action Mechanisms and Mode of Trypsin Inhibitors: A Systematic Review. In *Journal of Enzyme Inhibition and Medicinal Chemistry*; Taylor and Francis Ltd., 2022; pp 749−759 DOI: 10.1080/14756366.2022.2039918.

https://doi.org/10.1021/acsami.2c17531
ACS Appl. Mater. Interfaces 2022, 14, 52553−52565